Matter

CellPress

Article

Soft Matter Mechanics and the Mechanisms Underpinning the Infrared Vision of Snakes

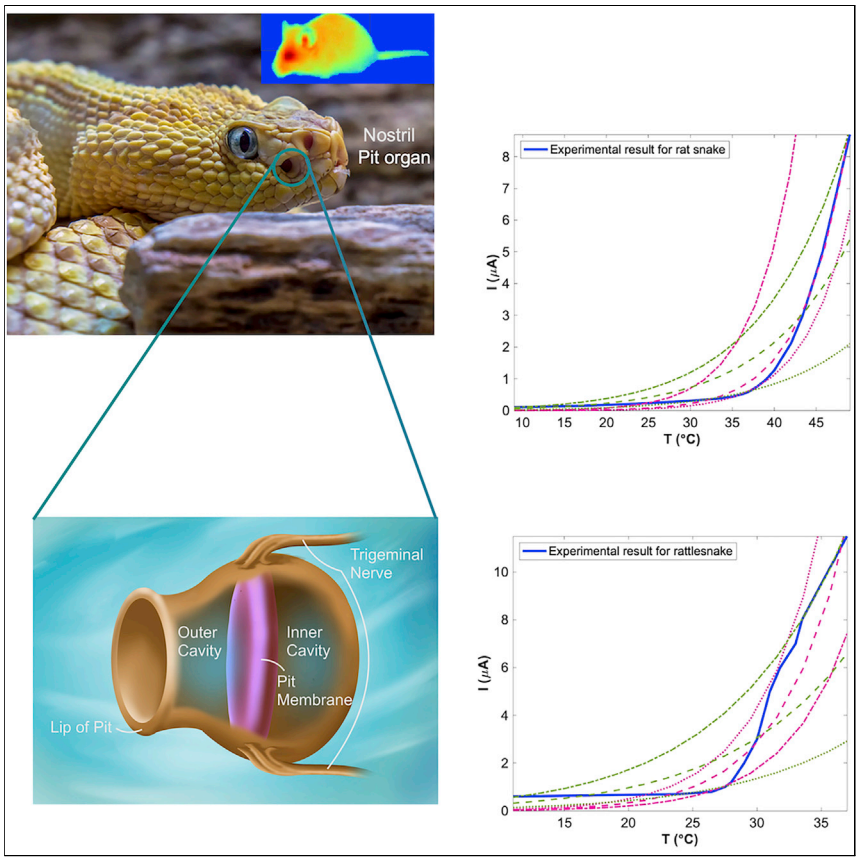

Elucidation of the mechanism underpinning the infrared vision of the pit-bearing snakes (vipers, pythons, and boas) has remained an open problem. In this paper, we propose that the cells in the snakes' pit membrane organ behave like an apparent pyroelectric material to allow transduction of heat radiation into electricity. Our model is able to explain most of the quantitative and qualitative experimental observations.

Faezeh Darbaniyan, Kosar Mozaffari, Liping Liu, Pradeep Sharma

psharma@uh.edu

HIGHLIGHTS

The mechanism underpinning the heat vision of pit-bearing snakes is introduced

Snake pit membrane cells are responsible for converting heat into electrical signals

Our model shows thermoelectric transduction and captures key elements of the phenomenon

The model shows excellent qualitative and quantitative comparison with known experiments

3 **Understanding**
Dependency and conditional studies on material behavior

Darbaniyan et al., Matter 4, 1–12
January 6, 2021
https://doi.org/10.1016/j.matt.2020.09.023

Please cite this article in press as: Darbaniyan et al., Soft Matter Mechanics and the Mechanisms Underpinning the Infrared Vision of Snakes, Matter (2020), https://doi.org/10.1016/j.matt.2020.09.023

Matter

CellPress

Article

Soft Matter Mechanics and the Mechanisms Underpinning the Infrared Vision of Snakes

Faezeh Darbaniyan,[1] Kosar Mozaffari,[1] Liping Liu,[2] and Pradeep Sharma[1,3,*]

SUMMARY

Pit-bearing snakes (vipers, pythons, and boas) have the extraordinary ability to "see" and accurately locate their prey and predators in total darkness. These animals use the infrared radiation emanating from objects that are warmer relative to the background environment to form a thermal image. Although enormous progress has been made to identify the key physiological features that enable the infrared vision of these snakes and a few other animals, the precise thermoelectric transduction mechanism that mediates the conversion of infrared heat to processable electrical signals has remained elusive. In this work, we quantitatively outline how cells in the snake's pit membrane organ act as apparent pyroelectric materials and convert infrared radiation into electrical signals. Despite the exceptional simplicity of our proposed mechanism and model, we are able to explain many central experimental results pertaining to the transduction process.

INTRODUCTION

All mammals have warmth receptors. This is a necessary evolutionary ability that permits us (and other animals) to differentiate hot from cold. However, reminiscent of the extraterrestrial from the iconic movie *Predator*, certain animals, such as pit vipers (Crotalinae), Pythoninae, Boinae of the Boidae, vampire bats, some species of insects, and others, can generate a *thermal image* of entities that are warmer than the ambient medium and, in coordination with their optical apparatus, possess vision of unnerving accuracy even in total darkness (Figure 1A).[1–4] The sensitivity of snakes' heat vision is extraordinarily precise (on the order of milli-Kelvin temperature difference) and surpasses the responsiveness of the best human-made sensors. As an example, an animal warmer by 10°C compared with the ambient temperature that makes only a fleeting appearance (a mere half a second) at a distance of 40 cm can be detected by pit vipers.[5]

Decades of experiments and analysis have implicated the pit organs in the heat-vision-capable snakes as playing a central role in infrared (IR) radiation detection. The pit organ is a hollow chamber enclosed by a thin membrane and is purported to act as an "antenna" for IR light[7] (Figure 1B). It is located between the eye and the nostril on both sides of the face of Crotalinae (Figure 1A) and is distributed over the snout of pythons and boas.[8,7] The mechanistic explanation for the IR vision has been sought from various viewpoints: the geometry and morphology of the pit organ structure, neural processing, and proteins such as TRPA1, among others. The IR vision in snakes exhibits several idiosyncratic features, of which two of the notable ones are (1) an acute sensitivity to rapid temperature changes and a virtual unresponsiveness to steady-state temperature and (2) heightened response upon initial contact and rapid dissipation of the response upon prolonged interaction.[5,9,10]

Progress and Potential

Certain animals, such as pit-bearing snakes, are able to form a thermal image of heat-generating prey in complete darkness, analogous to infrared night goggles. What is the biophysical mechanism that permits such an extraordinary ability? In this work, we seek to provide an answer to this enduring mystery. We show that biological cells universally behave as pyroelectric materials and thus can convert heat into electrical signals. The "apparently" pyroelectric cells, coupled with the pit organ apparatus of snakes and other physiological features, endow these animals with the ability to detect heat radiation.

Please cite this article in press as: Darbaniyan et al., Soft Matter Mechanics and the Mechanisms Underpinning the Infrared Vision of Snakes, Matter (2020), https://doi.org/10.1016/j.matt.2020.09.023

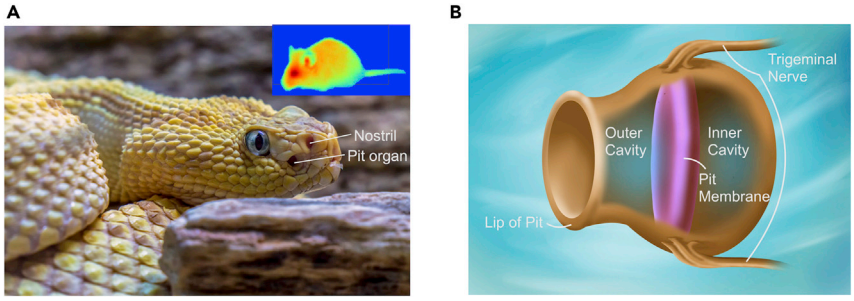

Figure 1. Pit Viper and a Schematic of the Pit Organ of a Rattlesnake

(A) Pit viper: a schematic picture of an infrared image of prey formed in its brain. (B) Rattlesnake's pit organ. The rattlesnake's pit organ is a thin membrane stretched between the inner and the outer cavities that is responsible for intercepting infrared radiation.[6]

In typical electrophysiological studies, the electric current from the heat-activated pit membrane is monitored under various conditions of radiation stimuli, and the functional properties of the organs have been characterized.[7,11] Significant progress was made when an analysis of pit-bearing snakes revealed that the pit organs of these vertebrates have nerve fibers richer in TRPA1 protein than the other non-pit snakes. In this study, the TRPA1 channels were identified as the potential reason for IR radiation sensation.[12,13] The rich literature on this topic points to a rather complex phenomenology underpinning IR vision, and a multitude of physiological features no doubt conspire together to achieve such an ability. For example, regarding the pit organ structure, having a thin membrane in between two cavities that has a very low thermal conductance[14] (as a result of its porous structure)[15] results in enhanced conservation of heat and rapid warming. The energy does not easily dissipate to other parts. Germane to the TRPA1 channels, they are voltage-gated ion channels and even a small temperature change leads to an increased opening rate and an increased current carried by Ca^{2+} ions.[16] However, in all such studies, whether they are concerned with the morphology of the pit organ or the surface structure of the IR receptors, the neural pathways of IR perception or the role of protein channels such as TRPA1, an explanation for the central transduction mechanism permitting the conversion of the IR signature into processable electrical signals is missing.

The presence of a so-called *pyroelectric* material would explain the transduction experiments. Notably, human-made IR detectors indeed employ pyroelectric materials. In such materials, a temperature variation can cause an electrical polarization. However, this phenomenon is observed only in certain classes of hard, low-symmetry crystalline materials, and no such material has ever been found in any of the IR-receptive animals.[5,9,17]

In this work, we theoretically prove that a biological membrane with a pre-existing electrical field (or frozen/stabilized charges) behaves like a pyroelectric material whose strength mainly depends on its thermal expansion property and the amount of pre-existing electric field/charge density (Figure 2). Our model provides the missing link to explain the conversion of IR radiation into electricity for the specific case of pit-bearing snakes. The developed model is qualitatively and quantitatively able to explain nearly all the key experimental results on IR reception.

PHYSICAL AND MATHEMATICAL MODEL

In this section, we briefly summarize the mathematical model and the pertinent governing equations. We specialize our equations to a simplified 1D model for the cell membrane, since the key physics is readily captured by this approximation.

[1]Department of Mechanical Engineering, University of Houston, Houston, TX 77204, USA

[2]Department of Mathematics and Department of Mechanical & Aerospace Engineering, Rutgers University, New Brunswick, NJ 08854, USA

[3]Department of Physics, University of Houston, Houston, TX 77204, USA

*Correspondence: psharma@uh.edu

https://doi.org/10.1016/j.matt.2020.09.023

Please cite this article in press as: Darbaniyan et al., Soft Matter Mechanics and the Mechanisms Underpinning the Infrared Vision of Snakes, Matter (2020), https://doi.org/10.1016/j.matt.2020.09.023

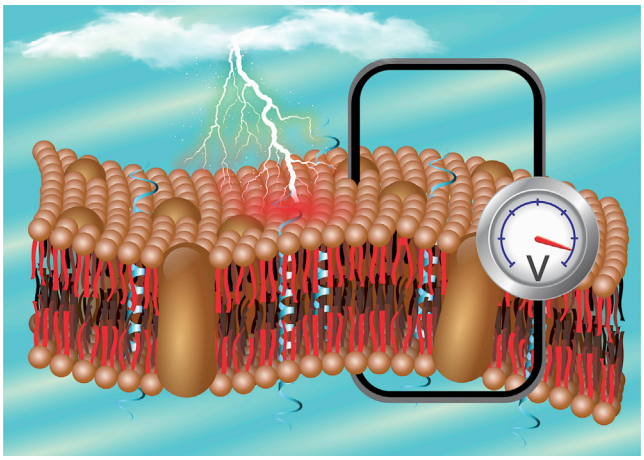

Figure 2. Schematic Illustration of a 2D Membrane Subjected to Heat Radiation and the Consequent Change in Electrical Field across Its Thickness

Governing Equations

The details of the derivation are recorded in the Supplemental Information. We sketch out only the key elements in what follows. The position of the material point in the reference (Ω_R) and spatial (Ω_t) configurations is specified by Lagrangian coordinates $\mathbf{X}\in\Omega_R$ and Eulerian coordinates $\mathbf{x}\in\Omega_t$, respectively. Operators ∇ and $\nabla\cdot$ (resp. $\nabla_\mathbf{x}$ and $\nabla_\mathbf{x}\cdot$) are the gradient and divergence taken with respect to the Lagrangian coordinates $\mathbf{X}$ (resp. Eulerian coordinates $\mathbf{x}$) accordingly. We denote by $\mathbf{F}=\nabla\mathbf{x}$ the deformation gradient, by $\mathbf{C}=\mathbf{F}^T\mathbf{F}$ the right Cauchy-Green tensor, and by $J=\det\mathbf{F}$ the Jacobian of the deformation gradient. With the assumption of thermoelastic incompressibility (as we made in our prior work),[18] we have:

$$J = 1+3\alpha\Delta T, \qquad \text{(Equation 1)}$$

where α is the linear thermal expansion coefficient and $\Delta T = T - T_0$ is the temperature change of the system from the reference temperature, T_0. Defining $\mathbf{d}$ as the electric displacement in the current configuration, the Maxwell equations of electrostatics are:

$$\nabla_\mathbf{x}\cdot\mathbf{d}=\frac{\rho_e}{J} \quad \text{in } \Omega_R, \qquad \text{(Equation 2)}$$

where ρ_e is the external charge density. Setting ε as the electric permittivity of the material, we have $\mathbf{d} = \varepsilon\mathbf{e}$. In the absence of body force we have:

$$\begin{aligned}\nabla\cdot\boldsymbol{\sigma}&=0 \quad \text{in } \Omega_R,\\ \boldsymbol{\sigma}\cdot\mathbf{n}&=\tilde{\mathbf{t}}^e \quad \text{on } \partial\Omega_R,\end{aligned} \qquad \text{(Equation 3)}$$

where $\tilde{\mathbf{t}}^e$ is the surface traction, $\mathbf{n}$ is the unit outward vector, and $\boldsymbol{\sigma}$ is the total mechanical and electrical stress in the system (Supplemental Information):

$$\begin{aligned}\boldsymbol{\sigma} = \mu\mathbf{F} - \Pi J\mathbf{F}^{-T} - \frac{\varepsilon}{2}J\left|\mathbf{F}^{-T}\nabla\xi\right|^2\mathbf{F}^{-T}\\ +\varepsilon J\left(\mathbf{F}^{-T}\nabla\xi\right)\otimes\left(\mathbf{C}^{-1}\nabla\xi\right),\end{aligned} \qquad \text{(Equation 4)}$$

where μ is the shear modulus, Π is the Lagrange multiplier to conserve thermoelastic incompressibility, and ξ is the electric potential. The temperature evolution obeys the following equation (Supplemental Information):

$$C\dot{T} + 3\alpha T\dot{\Pi} = r_e + \nabla\cdot(k\nabla T), \qquad \text{(Equation 5)}$$

Please cite this article in press as: Darbaniyan et al., Soft Matter Mechanics and the Mechanisms Underpinning the Infrared Vision of Snakes, Matter (2020), https://doi.org/10.1016/j.matt.2020.09.023

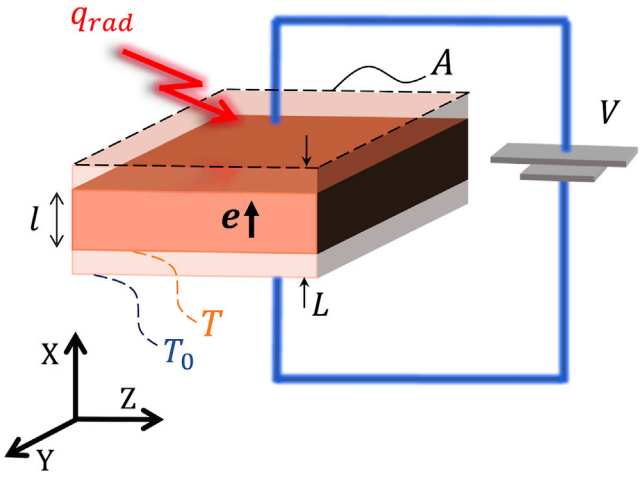

Figure 3. Schematic of the Simplified One-Dimensional Model of the Neuronal Cell Membrane in the Snake Pit Organ

Here q_{rad} is the heat radiation, A is the area of the thermal detector, L and l respectively denote the initial (before consideration of voltage difference and radiation heat) and final thickness, and T_0 and T are their corresponding temperatures. The voltage difference along the thickness of the cell membrane is assumed to be a constant, V, and the consequent electric field, $\boldsymbol{e}$, varies with the change in membrane thickness.

where $\dot{-} = \frac{d}{dt}$ denotes the time derivative, and C, k, and r_e are, respectively, the specific heat capacity per unit volume, the thermal conductivity, and the radiation power per unit area of radiating surface, per unit wavelength.

One-Dimensional Electret Model for Cells in the Pit Organ and Their Pyroelectric Behavior

We assume that the neuronal cell membrane in the pit organ can be treated as a thin film (Figure 3) and can be treated as a 1D electret or equivalently a thin film with a pre-existing voltage. Within this assumption, q_{rad} is the heat radiation emanating from the prey (or a relevant object), A is the area of the thermal detector (area of membrane facing the IR radiation), L and l denote the electret initial (before applying voltage difference and radiation heat) and final thickness, and T_0 and T are their corresponding temperatures. Voltage difference across the membrane thickness is assumed to be constant and denoted by V, and consequently the current electric field, $\boldsymbol{e}$, just varies with the change in thickness of the membrane.

The mechanical and electrostatic boundary conditions on the upper, S_u, and lower, S_l, surfaces are set as:

$$\tilde{\mathbf{t}}^e = 0, \quad \xi(\mathbf{X}, t) = \xi_b(\mathbf{X}, t) \quad \text{on } S_u \cup S_l. \qquad \text{(Equation 6)}$$

Here, the prescribed voltages are $\xi_b = V$ on the upper surface S_u and $\xi_b = 0$ on the lower surface S_l. For the traction-free system illustrated in Figure 3, Equation 4 results in:

$$\sigma_{xx} = \mu\Lambda - \Pi\frac{J}{\Lambda} + \frac{\varepsilon}{2}\frac{J}{\Lambda}e^2 = 0,$$
$$\sigma_{yy} = \sigma_{zz} = \mu\sqrt{\frac{J}{\Lambda}} - \Pi\sqrt{J\Lambda} - \frac{\varepsilon}{2}e^2\sqrt{J\Lambda} = 0, \qquad \text{(Equation 7)}$$

where σ_{xx} (resp. σ_{yy} and σ_{zz}) is the normal stress in the X (resp. Y and Z) direction, $\Lambda = \frac{l}{L}$ is the stretch of electret along the thickness direction, and e is the magnitude of

Please cite this article in press as: Darbaniyan et al., Soft Matter Mechanics and the Mechanisms Underpinning the Infrared Vision of Snakes, Matter (2020), https://doi.org/10.1016/j.matt.2020.09.023

electric field shown in Figure 3. (Here, we consider that we have equal dimensions in the Y and Z directions for a 1D electret.) Zero traction in the plane directions ($\sigma_{yy} = \sigma_{zz} = 0$) yields the Lagrange multiplier as $\Pi = \frac{\mu}{\Lambda} - \frac{\varepsilon}{2}e^2$. Substituting Π, J, and e in σ_{xx} gives:

$$\sigma_{xx} = \mu\left(\Lambda - \frac{(1+3\alpha\Delta T)}{\Lambda^2}\right) + \frac{\varepsilon(1+3\alpha\Delta T)}{\Lambda}\left(\frac{V}{\Lambda L}\right)^2 = 0. \quad \text{(Equation 8)}$$

Before applying radiation heat, we have $\sigma_{xx} = \mu\left(\Lambda_0 - \frac{1}{\Lambda_0^2}\right) + \frac{\varepsilon}{\Lambda_0}\left(\frac{V}{\Lambda_0 L}\right)^2 = 0$. Here Λ_0 is the stretch caused by applied voltage and $\Lambda = \Lambda_0(1 + \alpha\Delta T)$ is the final stretch of the electret as a result of both radiation heat and applied voltage. Substituting Λ in Π, considering constant prescribed voltages, and differentiating with respect to time, we obtain:

$$\dot{\Pi} = \frac{-\mu\alpha\dot{T}}{\Lambda_0(1+\alpha\Delta T)^2} + \frac{V^2}{L^2}\frac{\varepsilon\alpha\dot{T}}{\Lambda_0^2(1+\alpha\Delta T)^3}. \quad \text{(Equation 9)}$$

Equation 5 for the 1D structure illustrated in Figure 3, with $r_e = \epsilon q_{\text{rad}}$, with ϵ being the emissivity of the material (the ratio of energy radiated by the material to energy radiated by a blackbody at the same temperature) and q_{rad} the radiation heat glowing the pit membrane, becomes:

$$C^*\dot{T} - k\nabla^2 T = \epsilon q_{\text{rad}}, \quad \text{(Equation 10)}$$

where

$$C^* = C - \frac{3\mu\alpha^2 T}{\Lambda_0(1+\alpha\Delta T)^2} + \frac{3\varepsilon\alpha^2 V^2 T}{(\Lambda_0 L)^2(1+\alpha\Delta T)^3}, \quad \text{(Equation 11)}$$

is the effective heat capacity of the system.

Considering q as the induced electric charge density (electric charge per unit area) at the upper surface of the electret and d as the electric displacement inside the electret, the Maxwell equation, Equation 2, implies that $0 - d = q$. From the definition of electric displacement, $d = \varepsilon e$, with ε and e being the material's electric permittivity and the magnitude of electric field inside the membrane, we obtain $q = -\varepsilon e$. The pyroelectric coefficient can also be defined as $p = dq/dT$, which yields $p = -\varepsilon\frac{de}{dT}$. Substituting $e = \frac{V}{l}$ for constant electric potential and variable length, $l = \Lambda L$, we obtain:

$$p = \frac{\varepsilon V}{\Lambda^2 L}\frac{d\Lambda}{dT},$$

and substituting $\Lambda = \Lambda_0(1 + \alpha\Delta T)$, we obtain:

$$p = \frac{\varepsilon\alpha V}{\Lambda_0 L(1+\alpha\Delta T)^2}. \quad \text{(Equation 12)}$$

Infrared Detection

When IR radiation is detected, the pit organ mediates the transmittal of the heat to the neuronal membrane that will change to a temperature of $T_0 + \Delta T$. This change in temperature for the 1D system shown in Figure 3 can be found by solving the heat-balance equation, Equation 10. If we assume that the incident thermal flux is a periodic function, then:

$$q_{\text{rad}} = r_0 e^{i\omega t}, \quad \text{(Equation 13)}$$

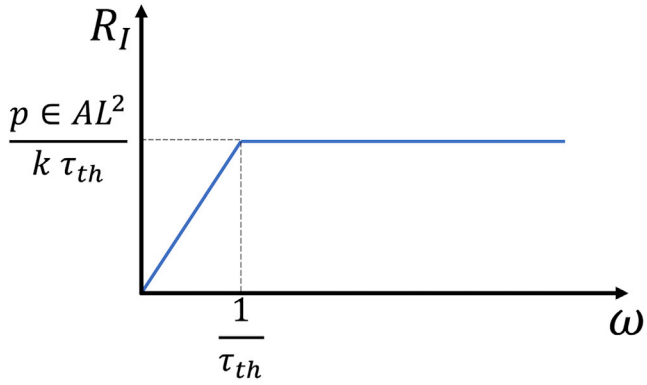

Figure 4. Responsivity Plot versus Heat Signal Frequency

where r_0 is the amplitude of the incident sinusoidal flux and ω is the frequency of the signal. The simplified solution of Equation 10, by assuming $\nabla^2 T = \Delta T/L^2$, may be easily obtained by removing the transient part:[19]

$$\Delta T = \frac{\epsilon r_0 L^2}{\sqrt{k^2 + (\omega C^* L^2)^2}}. \qquad \text{(Equation 14)}$$

The change in temperature, ΔT, can also be manipulated into a more useful term called electric responsivity, R_I, which is the electrical output of the detector divided by the incident thermal flux:[20]

$$R_I = \frac{I}{r_0}. \qquad \text{(Equation 15)}$$

We define the thermal response time as:

$$\tau_{th} = \frac{C^* L^2}{k}. \qquad \text{(Equation 16)}$$

From the definition of the pyroelectric coefficient and thermal response time we obtain:

$$I = p\omega A \Delta T = \frac{p\epsilon\omega r_0 A L^2}{k\sqrt{1+\omega^2\tau_{th}^2}}. \qquad \text{(Equation 17)}$$

And from Equations 15 and 17, the responsivity plot versus heat signal frequency can be schematically depicted by Figure 4.

Evidently, if $\omega > \frac{1}{\tau_{th}}$, the responsivity does not change significantly, and at low frequencies the electric current generated is insignificant. From Planck's law, the incident flux per unit area, characterized by the wavelength λ that emanates from a hot body at temperature T with area A_h, inclined by receptor with angle β,[20] located at a distance of R, is:

$$r_0 = \frac{2hc^2 A_h \cos\beta}{\lambda^5 (e^{hc/\lambda k_B T} - 1) R^2}, \qquad \text{(Equation 18)}$$

where h is Planck's constant ($6.626 \times 10^{-34}[J.s]$), c is the speed of light in the medium ($2.998 \times 10^8[m/s]$), and k_B is the Boltzmann constant ($1.381 \times 10^{-23}[J/K]$). Substituting incident flux, Equation 18, in electric current, Equation 17, for the case in which $\omega \gg \frac{1}{\tau_{th}}$ and $\beta = 0$ simplifies to:

Please cite this article in press as: Darbaniyan et al., Soft Matter Mechanics and the Mechanisms Underpinning the Infrared Vision of Snakes, Matter (2020), https://doi.org/10.1016/j.matt.2020.09.023

$$I = \frac{2hc^2 p\epsilon A A_h L^2}{\tau_{th} k R^2 \lambda^5 \left(e^{hc/\lambda k_B T} - 1\right)}. \quad \text{(Equation 19)}$$

RESULTS AND DISCUSSION

In this section, to the extent possible, we attempt to reconcile experimental observations with our model.

Material Properties and Extraction of Model Parameters from Phenomenological Observations

Our model requires several inputs primarily related to the material properties of the cellular structure in the pit organ. Like most biophysical problems, we face uncertainty in the precise values of the model parameters. However, taking cognizance of the phenomenological observations, we can certainly make estimates of the range of these parameters, which we proceed to do in this section.

Venomous pit vipers detect warm-blooded prey through their ability to sense IR radiation in the range of 50 nm to 1 mm wavelength[3] and this translates to a detectable frequency range of 1.8 THz to 2.5 PHz.[3] The whole pit organ thickness is reported to vary from 10 to 15 μm, with an area of about 30 mm^2. Substituting typical values relevant for a boa constrictor into Equation 18, we obtain $7.07 \times 10^{-6} < \frac{A_h \cos\beta}{R^2} < 1.24 \times 10^{-5}$. This means that if a prey faces a boa ($\beta = 0$) at a distance of 40 cm,[5] then $1.13\ mm^2 < A_h < 1.98\ mm^2$, which is in the range of the typical area of a boa's pit opening and also yields the limit of the area of the heat source area facing the prey that can be detected.

For rattlesnakes and pythons, considering $\lambda = 10\ \mu m$ (since the black-body radiation from a typical prey mammal or bird for most of these snakes occurs at this wavelength)[21] and using Equation 18, we estimate $\frac{A_h \cos\beta}{R^2} \sim 2.88 \times 10^{-9}$ for a diamondback rattlesnake and $\frac{A_h \cos\beta}{R^2} \sim 3.3 \times 10^{-8}$ for a ball python. This implies that such snakes, at the corresponding distance (of 100 cm for rattlesnakes and 30 cm for pythons), are able to detect prey facing the snake with $A_h \sim 0.003\ mm^2$. This is consistent with physiological measurements.

The temperature change, ΔT, which is sufficient to raise the firing rate of the trigeminal nerve, has been estimated to be 0.002°C and 0.003°C for boas and rattlesnakes, respectively.[5,6,9] The density of a cell membrane is about 1300 kg/m^3,[22] and its heat capacity, varying by temperature change, is in the range of 600 J/kg°C < C < 2250 J/kg°C.[23,24] Neglecting the temperature dependence of the heat capacity, we assume C = 1050 J/kg°C. The thermal conductivity of pit organ is quite low, k = 0.11 W/m°C, which results in a significant local temperature gradient around the receptor areas. From a mechanical viewpoint, the cell membrane elastic modulus in its thickness direction is estimated to be 40 MPa.[25] Although we are not aware of precise measurements of cellular thermal expansion for the neuronal cells in the pit organ, we estimate the areal thermal expansion coefficient at room temperature to be $10.6 \times 10^{-3}/°C$,[26] whereas its linear thermal expansion coefficient likely falls in the order of $3 \times 10^{-3}/°C$.[27]

Experiments on boa constrictors have shown that they can detect power densities from 8 to 14 mW/cm^2 from a CO_2 laser with 10.6 μm wavelength emanating from a distance of about 40 cm.[5,17] Diamondback rattlesnakes and ball pythons can respectively detect preys up to 100 and 30 cm away, with irradiance contrast of 3.35×10^{-6} and 3.83×10^{-5} W/cm^2, respectively.[3] (Irradiance is the radiant flux received by a surface or the flux that is incident on the surface. The irradiance unit

Please cite this article in press as: Darbaniyan et al., Soft Matter Mechanics and the Mechanisms Underpinning the Infrared Vision of Snakes, Matter (2020), https://doi.org/10.1016/j.matt.2020.09.023

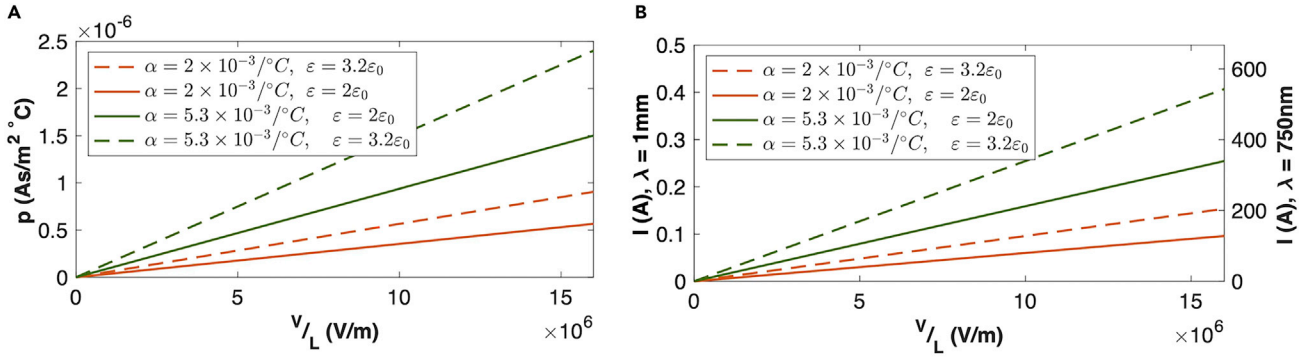

Figure 5. Variation in Pyroelectric Coefficient and Electric Current in the Pit Cell Membrane with Respect to the Electric Field along the Thickness

Variation in (A) pyroelectric coefficient and (B) electric current in the pit cell membrane with respect to the electric field along the thickness. The electric field varies from 0 to the maximum value reported for rattlesnakes ($V = 80$ mV[7] and $L = 5$ nm). Graphs were generated for maximum and minimum values of thermal expansion coefficient and dielectric constant, and shear modulus of membrane was set to be 13.3 MPa.[14,26–28] For plotting (B), temperature change was set to be 0.003°C according to Newman and Hartline,[6] and right and left *y* axes denote the value of electric current for minimum and maximum of heat radiation wavelength sensible by pit vipers.[3]

is determined as power per unit area. There is a clear relationship between irradiance and distance. As the distance between the radiation source increases, the irradiance decreases.) Finally, the voltage difference across the pit organ of the rattlesnake and the rat snake is about 80 mV,[7] and in subsequent calculations, we will take the relative dielectric constant of membranes to vary from 2 to 3.2.[28]

Typical Values for the Pyroelectric Coefficient of Cells in the Pit Organ and Generated Electric Current

Prior to comparison with experiments, it is instructive to examine the range of values our model predicts for some key quantities such as the apparent pyroelectric coefficient, membrane stretch, and generated electric current for a typical thermal stimulus. Under Material Properties and Extraction of Model Parameters from Phenomenological Observations, we used the following estimates for the parameters of cell membrane of pit organ: relative dielectric constant, $2<\varepsilon/\varepsilon_0<3.2$; shear modulus, $\mu \approx 13.3$ MPa; and thermal expansion coefficient, $2 \times 10^{-3}/°C<\alpha<5.3 \times 10^{-3}/°C$. Using a transmembrane voltage difference of $V = 80$ mV, and its thickness as $L = 5$ nm, the electric field along the cell membrane thickness can be estimated to go as high as 16 MV/m. Substituting the highest and lowest values of the aforementioned parameters in Equation 8 we obtain the membrane's stretch, and from Equation 12, the calculated pyroelectric coefficient is plotted in Figure 5A. Consistent with our proposed mechanism based on the notion of electrets, the pyroelectric coefficient depends on the pre-existing transmembrane voltage. Setting $A = 30$ mm^2 and $\Delta T = 0.003$°C from Newman and Hartline[6] and substituting it together with highest and lowest wavelengths reported in Equation 17, we obtain Figure 5B. As evident from Figure 5A, the pyroelectric coefficient can be as high as 2.5 μAs/m^2°C. From Figure 5B, especially for low radiation wavelengths, a snake can generate significant electric current as a result of the pyroelectric effect, the values for which fall within the range of the electrophysiological measurements (see next section).

Comparison of Model with Experimental Electric Current Measurements

In Figure 6B we plot the normalized electric current (the normalization is with respect to the value of current at $T = 45$°C) versus heat source temperature. The gray lines indicate the theoretical results, i.e., Equation 19, for different wavelengths that were reported to be detected by the snakes,[3] and the colored lines are from experiments performed on

Please cite this article in press as: Darbaniyan et al., Soft Matter Mechanics and the Mechanisms Underpinning the Infrared Vision of Snakes, Matter (2020), https://doi.org/10.1016/j.matt.2020.09.023

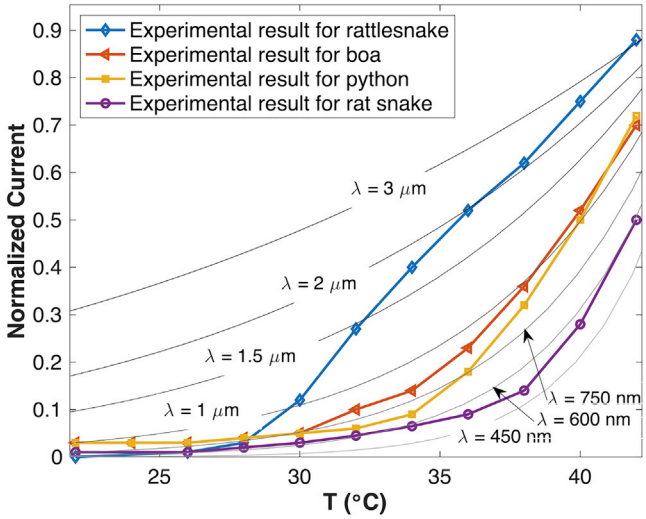

Figure 6. Normalized Electric Current with Respect to the Current at $T = 45^{\circ}C$ versus Temperature

The experimental results from Gracheva et al.[7] are compared with theory (Equation 19) for different wavelengths of infrared heat radiation. Our theoretical results are in gray and the experimental results are solid colored lines.

the four snakes.[7] As evident from our model and in agreement with the experiments,[7,9,17] snakes can detect only prey whose body temperature is above a specific threshold. The model also captures well the qualitative variation of the measured electric current with respect to the heat source temperature.

Figure 7 compares our theoretical and experimental results for rattlesnake and rat snake. Blue solid lines in Figures 7A and 7B are the experimental results for variation in electric current in rattlesnake and rat snake, with respect to the prey's body temperature.[7] Green and pink dashed lines in Figure 7 correspond to our model, Equation 19, for λ = 1.4 μm and λ = 750 nm. As evident, the model's *quantitative* agreement with the experiments on rat snakes is stronger and arguably not so much for rattlesnakes. On this note, we simply point out that our agreement is reasonable *qualitatively* (for both), but there are many experimental details that we do not know and arguably several details that our model probably does not account for. This accounts for the less than perfect quantitative comparison in certain cases.

Responsivity

The idiosyncratic responsivity of snakes' detection of thermal stimuli is an important aspect for any model to capture. To that end, we calculate the value for thermal response time, τ_{th}, and compare $1/\tau_{th}$ with frequencies detectable by snakes. Substituting material properties from Material Properties and Extraction of Model Parameters from Phenomenological Observations into Equation 16 yields the minimum value of thermal response time as $\tau_{th} = 3.1 \times 10^{-10}$s, which gives the maximum inverse as $1/\tau_{th} = 3.2 \times 10^{9}/s$, which is much lower than the minimum frequency detectable by pit-bearing snakes, 1.8 THz. Hereby the responsivity for the snake may be approximated by $R_I = p\epsilon AL^2/(k\tau_{th})$. As indicated earlier, this is consistent with the observations that snakes cannot detect low-frequency heat signals.

Figure 8 illustrates the variation in responsivity with respect to the frequency of the heat signal for rattlesnake (with material properties highlighted under Material

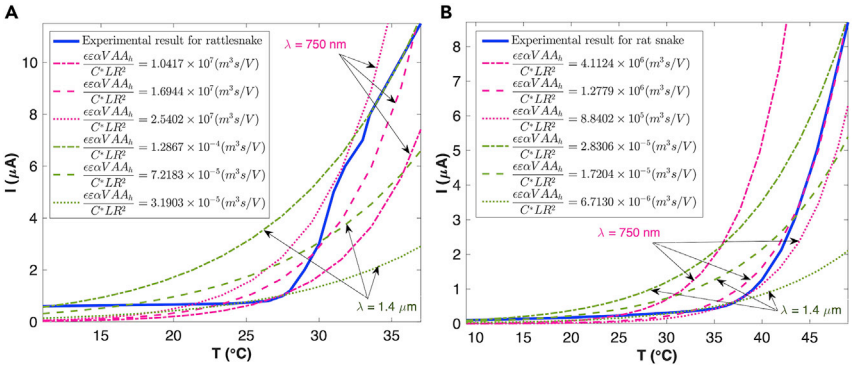

Figure 7. Variation in Electric Current with Respect to Temperature for Two Different Heat Radiation Wavelengths

(A) is compared with experimental results for rattlesnake and (B) is compared with rat snake results.[7]

Properties and Extraction of Model Parameters from Phenomenological Observations).

CONCLUDING REMARKS

The mechanistic underpinnings of the heat vision of animals like snakes requires accounting for several aspects, such as the morphology and thermal behavior of the pit organ; the surface structure of the IR receptors; the neural pathways of the IR perception, especially its link to how visual stimuli are employed, and the role of protein channels such as TRPA1. Our work, however, goes to the heart of what has endured as a key question: what is the mechanism that leads to the conversion of IR signature into an electrical signal? It has been speculated that the presence of a pyroelectric material would explain the thermoelectrical transduction mechanism; however, no such material has ever been discovered. We show, however, that a biological cell with a pre-existing transmembrane

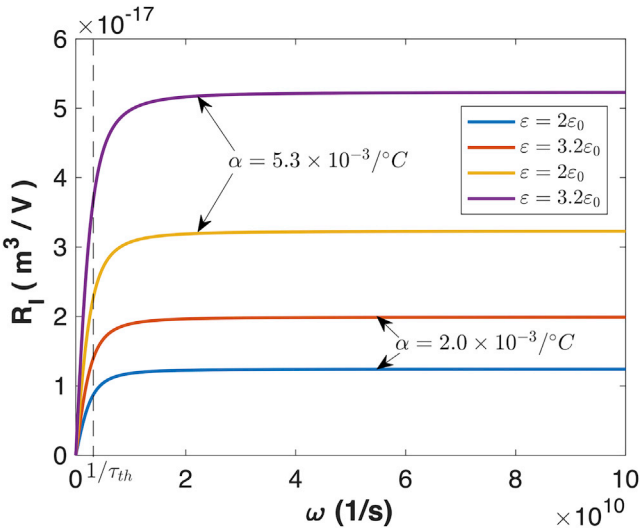

Figure 8. Variation in Responsivity of Pit Membrane with Respect to the Signal Frequency for Rattlesnake

The electric field was set to be 16 MV/m (since V = 80 mV[7] and L = 5 nm). Graphs were generated for maximum and minimum values of thermal expansion coefficient and dielectric constant and shear modulus of 13.3 MPa.[14,26–28] We assumed black-body radiation ϵ = 1, and we used heat capacity of C = 1050 J/kg°C[23,24] and membrane density of 1300 kg/m^3.[22]

electrical potential acts as a pyroelectric material. Coupled then with the other attributes of the heat-vision-possessing animals (e.g., the design of a pit organ, TRPA1 channels), this extraordinary sense is readily explained.

EXPERIMENTAL PROCEDURES

Resource Availability

Lead Contact

Pradeep Sharma (email: psharma@uh.edu).

Materials Availability

No new unique materials were generated in this study.

Data and Code Availability

All the necessary data for reproduction of the results have been provided in the main text. Additional data related to this paper can be obtained from the lead contact upon request.

SUPPLEMENTAL INFORMATION

Supplemental Information can be found online at https://doi.org/10.1016/j.matt.2020.09.023.

ACKNOWLEDGMENTS

P.S. would like to acknowledge the M.D. Anderson Professorship by the University of Houston. Discussions as well as a fruitful prior collaboration with Professor Kaushik Dayal on the topic of this paper are gratefully acknowledged.

AUTHOR CONTRIBUTIONS

Conceptualization & Methodology, P.S. and L.L.; Investigation, Visualization & Writing – Original Draft, F.D.; Validation & Writing – Review & Editing, K.M.; Supervision, P.S.

DECLARATION OF INTERESTS

The authors declare no competing interests.

Received: May 8, 2020
Revised: August 24, 2020
Accepted: September 24, 2020
Published: October 21, 2020

REFERENCES

1. Bullock, T.H., and Diecke, F. (1956). Properties of an infra-red receptor. J. Physiol. *134*, 47–87.

2. Campbell, A.L., Naik, R.R., Sowards, L., and Stone, M.O. (2002). Biological infrared imaging and sensing. Micron *33*, 211–225.

3. Ebert, J. (2007). Infrared sense in snakes–behavioural and anatomical examinations (crotalus atrox, python regius, corallus hortulanus), Ph.D. thesis, PhD Dissertation, Intitut für Zoologie (Rheinische Friedrich-Wilhelms).

4. Fang, J. (2010). Snake infrared detection unravelled. Nature. https://doi.org/10.1038/news.2010.122.

5. Lang, S.B. (2000). Piezoelectricity, pyroelectricity and ferroelectricity in biomaterials: speculation on their biological significance. IEEE Trans. Dielectrics Electr. Insul. *7*, 466–473.

6. Newman, E.A., and Hartline, P.H. (1982). The infrared "vision" of snakes. Sci. Am. *246*, 116–127.

7. Gracheva, E.O., Ingolia, N.T., Kelly, Y.M., Cordero-Morales, J.F., Hollopeter, G., Chesler, A.T., Sánchez, E.E., Perez, J.C., Weissman, J.S., and Julius, D. (2010). Molecular basis of infrared detection by snakes. Nature *464*, 1006.

8. de Cock Buning, T., Terashima, S.-i., and Goris, R.C. (1981). Python pit organs analyzed as warm receptors. Cell Mol. Neurobiol. *1*, 271–278.

9. Harris, J.F., and Gamow, R.I. (1971). Snake infrared receptors: thermal or photochemical mechanism? Science *172*, 1252–1253.

10. Lynn, W.G. (1931). The structure and function of the facial pit of the pit vipers. Am. J. Anat. *49*, 97–139.

11. Pappas, T.C., Motamedi, M., and Christensen, B.N. (2004). Unique temperature-activated neurons from pit viper thermosensors. Am. J. Physiology-Cell Physiol. *287*, C1219–C1228.

12. Yokoyama, S., Altun, A., and DeNardo, D.F. (2010). Molecular convergence of infrared vision in snakes. Mol. Biol. Evol. *28*, 45–48.

13. Geng, J., Liang, D., Jiang, K., and Zhang, P. (2011). Molecular evolution of the infrared sensory gene trpa1 in snakes and implications for functional studies. PLoS One *6*, e28644.

14. Gorbunov, V., Fuchigami, N., Stone, M., Grace, M., and Tsukruk, V. (2002). Biological thermal detection: micromechanical and microthermal properties of biological infrared receptors. Biomacromolecules *3*, 106–115.

15. Goris, R.C. (2011). Infrared organs of snakes: an integral part of vision. J. Herpetology *45*, 2–15.

16. R. Di Giacomo, L. Bonanomi, V. Costanza, B. Maresca, C. Daraio, Artificial Membranes Biomimicking Pit Vipers' Thermal Sensing.

17. Gamow, R.I., and Harris, J.F. (1973). The infrared receptors of snakes. Scientific Am. *228*, 94–101.

18. Darbaniyan, F., Dayal, K., Liu, L., and Sharma, P. (2019). Designing soft pyroelectric and electrocaloric materials using electrets. Soft Matter *15*, 262–277.

19. Rogalski, A. (2000). Infrared Detectors (netherlands).

20. Allard, M.E. (2007). Characterization of a Polymer-Based Mems Pyroelectric Infrared Detector, Tech. Rep (AIR FORCE INST OF TECH WRIGHT-PATTERSON AFB OH GRADUATE SCHOOL OF â€).

21. Gates, D.M. (1963). Energy exchange in the biosphere. Soil Sci. *96*, 76.

22. Paredes, A.M., Brown, D.T., Rothnagel, R., Chiu, W., Schoepp, R.J., Johnston, R.E., and Prasad, B. (1993). Three-dimensional structure of a membrane-containing virus. Proc. Natl. Acad. Sci. U S A *90*, 9095–9099.

23. Ivanova, V.P., and Heimburg, T. (2001). Histogram method to obtain heat capacities in lipid monolayers, curved bilayers, and membranes containing peptides. Phys. Rev. E *63*, 041914.

24. Grabitz, P., Ivanova, V.P., and Heimburg, T. (2002). Relaxation kinetics of lipid membranes and its relation to the heat capacity. Biophysical J. *82*, 299–309.

25. Krichen, S., Liu, L., and Sharma, P. (2017). Biological cell as a soft magnetoelectric material: elucidating the physical mechanisms underpinning the detection of magnetic fields by animals. Phys. Rev. E *96*, 042404.

26. Pencer, J., Nieh, M.-P., Harroun, T.A., Krueger, S., Adams, C., and Katsaras, J. (2005). Bilayer thickness and thermal response of dimyristoylphosphatidylcholine unilamellar vesicles containing cholesterol, ergosterol and lanosterol: a small-angle neutron scattering study. Biochim. Biophys. Acta *1720*, 84–91.

27. Marčelja, S. (1974). Chain ordering in liquid crystals: II. structure of bilayer membranes. Biochim. Biophys. Acta *367*, 165–176.

28. Gramse, G., Dols-Pérez, A., Edwards, M., Fumagalli, L., and Gomila, G. (2013). Nanoscale measurement of the dielectric constant of supported lipid bilayers in aqueous solutions with electrostatic force microscopy. Biophysical J. *104*, 1257–1262.